
TiCo: Transformation Invariance and Covariance Contrast for Self-Supervised Visual Representation Learning

Jiachen Zhu^{1*}Rafael M. Moraes³Serkan Karakulak²Vlad Sobol²Alfredo Canziani^{1,2}Yann LeCun^{1,2,4}¹Courant Institute, New York University²Center for Data Science, New York University³Viasat, Inc.⁴Facebook AI Research

Abstract

We present **Transformation Invariance and Covariance Contrast (TiCo)** for self-supervised visual representation learning. Similar to other recent self-supervised learning methods, our method is based on maximizing the agreement among embeddings of different distorted versions of the same image, which pushes the encoder to produce transformation invariant representations. To avoid the trivial solution where the encoder generates constant vectors, we regularize the covariance matrix of the embeddings from different images by penalizing low rank solutions. By jointly minimizing the transformation invariance loss and covariance contrast loss, we get an encoder that is able to produce useful representations for downstream tasks. We analyze our method and show that it can be viewed as a variant of MoCo [16] with an implicit memory bank of unlimited size at no extra memory cost. This makes our method perform better than alternative methods when using small batch sizes. TiCo can also be seen as a modification of Barlow Twins [35]. By connecting the contrastive and redundancy-reduction methods together, TiCo gives us new insights into how joint embedding methods work.

1 Introduction

The field of self-supervised visual representation learning has seen enormous progress in recent years. Most successful approaches fall into one of two classes: *pretext task* methods [31, 25, 36, 37, 10, 9, 21, 32, 24] or *joint embedding* methods [16, 5, 20, 4, 3, 15, 6, 35, 1]. Pretext task methods involve training a network to solve a pretext task and using the trained network to generate data representations for downstream tasks that we care about. A large number of pretext tasks have been proposed, with some of them reaching state-of-the-art performance at the time of publication. However, in the past year, multiple joint embedding methods were proposed and their performance surpassed the pretext task methods in almost all standard self-supervised benchmarks.

The joint embedding methods rely on the fact that good representations should be invariant to transformations that don't change the semantics of the inputs. Currently, the majority of joint embedding methods for visual representation learning use a stochastic data augmentation scheme to

*Correspondence to jiachen.zhu@nyu.edu

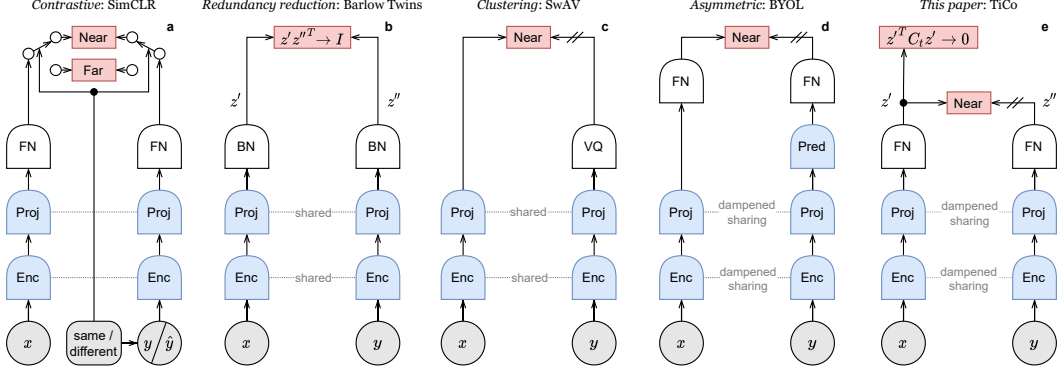


Figure 1: **Joint embedding learning categories and this paper’s contribution.** From left to right, an example of *contrastive learning*, *redundancy reduction*, *clustering-based*, *asymmetric network*, TiCo. Shaded circles \bigcirc represent observed variables, bullet shapes represent deterministic functions, dashed gray lines indicate (dampened) parameter sharing, // indicates a stop-gradient for backpropagation, • represents a bifurcation, and red boxes represent cost terms. **Contractions legend:** Enc: encoder, Proj: projector, Pred: predictor, FN: feature normalization, VQ: vector quantization, BN: batch normalization.

generate multiple distorted versions of the same image, and push the embeddings of those distorted images towards each other with the objective of making the representations invariant to those data augmentations. However, simply optimizing such an objective will result in a trivial solution where the encoder generates a constant representation for all inputs, since the constant representation is inherently invariant to any type of transformations in the input space. Therefore, different methods have been proposed to avoid having such a trivial solution, and they can roughly be summarized into four different categories: *contrastive learning methods* [5, 16, 20], *clustering-based methods* [3, 4], *asymmetric network methods* [15, 6] and *redundancy reduction methods* [35, 1], as shown in fig. 1.

In the present work, we introduce a novel method called TiCo, which also utilizes the joint embedding architecture. We discuss the details of the method in Section 3. Our method jointly optimizes both the transformation invariance objective and a covariance contrast objective, which effectively regularizes the covariance matrix of the embeddings. Interestingly, TiCo is both a contrastive learning method and a redundancy reduction method. On the one hand, it is equivalent to MoCo [16] with an altered contrastive loss that enables it to implicitly have an infinitely large memory bank without requiring extra memory, as we show in Section 3.2. This allows our method to achieve good performance without an explicit memory bank and use smaller batch sizes than required for other methods. On the other hand, TiCo can be considered to be the same as the Barlow Twins [35] with an exponential moving covariance matrix, which makes it a redundancy reduction method. We discuss the similarities in Section 3.3. We demonstrate the effectiveness of TiCo by testing its ability to learn useful representations from ImageNet images in Section 4. To the best of our knowledge, our work is the first to demonstrate the connection between contrastive learning and redundancy reduction methods. We argue that understanding this connection provides us with a new way to think about the joint embedding learning, which we explain in detail in Section 5.

2 Related Work

2.1 Contrastive Learning Methods

Contrastive learning methods [7, 22, 5, 16] maximize the agreement between representations of different augmentations of the same image while minimizing that of different images, as shown in fig. 1a. They are able to avoid the trivial solution, since having a constant representation for all images would mean that there is perfect agreement between the representations of different images. The challenge with contrastive learning methods is to find “hard” negative pairs that are close enough in the representation space to provide meaningful gradients. This can be addressed by using a large

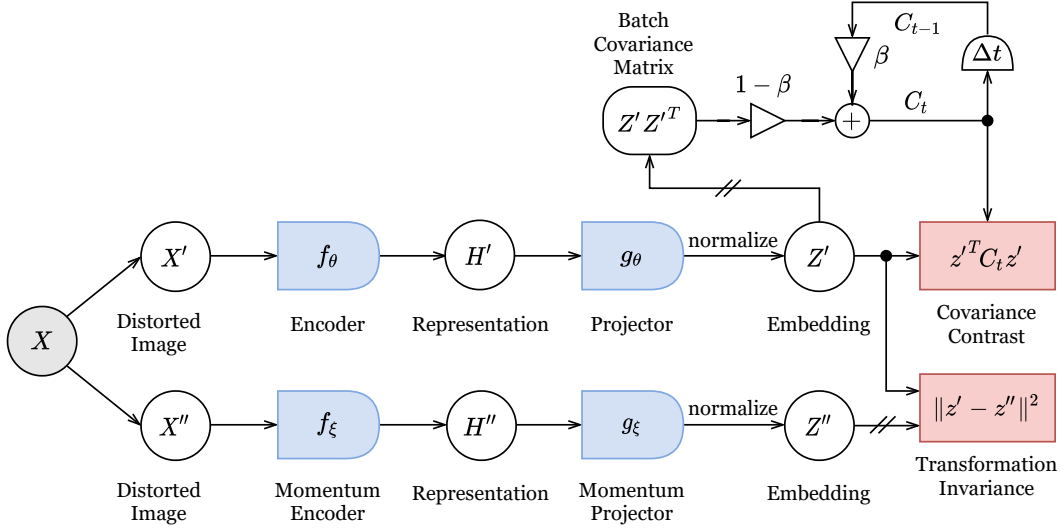


Figure 2: **TiCo architecture diagram.** Shaded circles \bullet represent observed variables, while empty circles \circ represent computed values, bullet shapes represent deterministic functions, // indicates a stop-gradient for backpropagation, \bullet represents a bifurcation, **red boxes** represent cost terms, Δ represents a multiplication by a scalar value, \oplus is an addition module, and Δt represents a unit time delay.

batch size [5], or by sampling negative pairs from representations stored in a memory bank [16]. Both of these solutions imply having a large memory footprint.

Contrastive Loss Function Many different contrastive loss functions have been proposed [7, 22, 29, 23, 26]. The reason why they are contrastive is because they compare negative and positive pairs of images, where the loss function yields a low value when two positive pairs are close together or two negative pairs are far apart, and a high value vice versa.

2.2 Redundancy Reduction Methods

Redundancy reduction methods, like Barlow Twins [35], regularize the covariance matrix of the embeddings to be close to the identity matrix while maximizing the agreement between different augmentations of the same image, as shown in fig. 1b. This formulation avoids having a constant trivial solution, since in that case any pair of components with an equal representation would be perfectly correlated, resulting in having maximum redundancy.

2.3 Other Joint Embedding Methods

Other approaches that recently have shown success in self-supervised representation learning employ clustering-based methods [3, 4] or asymmetric network methods [15, 5], shown in figs. 1c and 1d. While clustering based approaches make it easier to mine negative samples and eliminate the need to have a large batch size or a large memory bank, they introduce an additional clustering step that can be computationally expensive. Asymmetric network, like BYOL [15], have shown to have state-of-the-art performance while avoiding producing a constant representation. However, they are hard to analyze and it is not well understood how they avoid the trivial solution.

3 Method

3.1 TiCo Algorithm

Like other joint embedding methods, TiCo also operates on the embedding pairs of distorted images. Specifically, given a batch of n images $X = \{x_1, \dots, x_n\}$, two distorted views $X' = \{x'_1, \dots, x'_n\}$ and

$X'' = \{x''_1, \dots, x''_n\}$ are generated using a stochastic data augmentation \mathcal{T} . Then, we use two encoders f_θ and f_ξ and two projectors g_θ and g_ξ with parameters θ and ξ to generate the corresponding embeddings z'_i and z''_i , where $z'_i = g_\theta(f_\theta(x'_i))$, $z''_i = g_\xi(f_\xi(x''_i))$, and $z'_i, z''_i \in \mathbb{R}^d$. To simplify the notation, we assume that the outputs of the projector are normalized to unit vectors.

In our setting, we apply the same momentum encoder technique as proposed in MoCo [16], such that only the parameter θ is updated through backpropagation, and the parameters ξ is the exponential moving average of the parameter θ . At time step t , we have

$$\xi_t = \alpha \xi_{t-1} + (1 - \alpha) \theta_t \quad (1)$$

where $\alpha \in [0, 1]$ is a hyperparameter.

During training, we also keep an exponential moving average of the (non-centered) covariance matrix C_t of the embedding generated by the encoder f_θ and projector g_θ , such that, at time step t , C_t is updated using the following formula:

$$C_t = \begin{cases} \mathbf{0}, & t = 0 \\ \beta C_{t-1} + (1 - \beta) \frac{1}{n} \sum_{i=1}^n z'_i z'^T_i & \text{otherwise} \end{cases} \quad (2)$$

where $\beta \in [0, 1]$ is a hyperparameter.

The final loss function of TiCo has the following form:

$$\ell_{\text{TiCo}}(z'_1, \dots, z'_n, z''_1, \dots, z''_n) = \frac{1}{2n} \sum_{i=1}^n \|z'_i - z''_i\|^2 + \frac{\rho}{n} \sum_{i=1}^n z'^T_i C_t z'_i \quad (3)$$

$$= 1 - \frac{1}{n} \sum_{i=1}^n z'^T_i z''_i + \frac{\rho}{n} \sum_{i=1}^n z'^T_i C_t z'_i \quad (4)$$

where $\rho \in \mathbb{R}^+$ is a hyperparameter that controls the weight of the second term of the loss function.

Intuitively, the loss function jointly optimizes two objectives. The first term is trying to push the embeddings of different data augmentations of the same image closer to each other. The second term is trying to push each vector to the subspace of the covariance matrix with smaller eigenvalues. Therefore, we can decompose the loss function into two parts:

$$\ell_{\text{TiCo}}(z'_1, \dots, z'_n, z''_1, \dots, z''_n) = \underbrace{-\frac{1}{2n} \sum_{i=1}^n \|z'_i - z''_i\|^2}_{\text{transformation invariance}} + \underbrace{\frac{\rho}{n} \sum_{i=1}^n z'^T_i C_t z'_i}_{\text{covariance contrast}} \quad (5)$$

which gives us the name of our method: Transformation Invariance and Covariance Contrast. The pseudo code of the TiCo algorithm is shown in algorithm 1.

3.2 TiCo as a Contrastive Learning Method

To understand why TiCo is a contrastive learning method, let us first introduce the loss function used by TiCo, which is the squared contrastive loss function below:

$$\ell_{\text{Squared}}(z'_1, \dots, z'_n, z''_1, \dots, z''_n) = -\frac{1}{n} \sum_{i=1}^n z'^T_i z''_i + \frac{\rho}{n^2} \sum_{i=1}^n \sum_{j=1, j \neq i}^n \left(z'^T_i z''_j \right)^2 \quad (6)$$

Let us compare it to the popular InfoNCE contrastive loss function[22]:

$$\ell_{\text{InfoNCE}}(z'_1, \dots, z'_n, z''_1, \dots, z''_n) = -\frac{1}{n} \sum_{i=1}^n z'^T_i z''_i + \frac{\tau}{n} \sum_{i=1}^n \log \sum_{j=1}^n \exp \left(z'^T_i z''_j / \tau \right) \quad (7)$$

It is easy to see that, both loss functions pull the positive pairs together in the same way. However, the way they push negative pairs' embeddings away from each other is different. InfoNCE pushes z'_i and z''_j towards the opposite direction of each other to minimize the exponent, while the covariance contrast loss pushes those embeddings in orthogonal directions of each other. While there is just one direction which is the opposite direction of a given embedding, there are a large number of orthogonal directions in a high dimensional space. We hypothesize that this makes TiCo loss easier to optimize.

Algorithm 1: PyTorch-style pseudocode for TiCo

```
# f: encoder network (include both the encoder and projector) with parameter  $\theta$ 
# fm: momentum encoder network (include both the encoder and projector) with parameter  $\xi$ 
#  $\rho$ ,  $\alpha$  and  $\beta$ : hyperparameters
# n: batch size
# d: dimensionality of the embedding
# mm: matrix-matrix multiplication

for x in loader: # load a batch with n samples
    x_1, x_2 = augment(x) # two randomly augmented versions of x

    # compute embeddings
    z_1 = f(x_1) # nxd
    z_2 = fm(x_2) # nxd
    z_1 = F.normalize(z_1, dim=1) # normalize embeddings along the feature dimension
    z_2 = F.normalize(z_2, dim=1) # normalize embeddings along the feature dimension

    B = mm(z_1.T, z_1) / n # compute batch covariance matrix
    C =  $\beta C + (1 - \beta)B$  # update exponential moving covariance matrix

    loss = -(z_1 * z_2).sum(dim=1).mean() +  $\rho * (mm(z_1, C) * z_1).sum(dim=1).mean()$ 

    loss.backward()
    optimizer.step() # optimization step (only  $\theta$  is updated)

     $\xi = \alpha \xi + (1 - \alpha)\theta$  # update momentum encoder network (update  $\xi$ )
```

3.2.1 Combining MoCo with the Squared Contrastive Loss

Having introduced the squared contrastive loss function, we will now show TiCo's relation to the contrastive learning method MoCo [16].

First, let us substitute the InfoNCE loss used by MoCo with the squared contrastive loss function as below:

$$\ell_{\text{Squared}}(z'_1, \dots, z'_n, z''_1, \dots, z''_m) = -\frac{1}{n} \sum_{i=1}^n z_i'^T z_i'' + \frac{\rho}{nm} \sum_{i=1}^n \sum_{j=1}^m (z_i'^T z_j'')^2 \quad (8)$$

where m is the size of the memory bank. We have $m \geq n$ and $\{z''_{n+1}, \dots, z''_m\}$ are embeddings generated from previous steps and stored in the memory bank.

It is easy to see that this loss function can be rewritten as follows:

$$\ell_{\text{Squared}}(z'_1, \dots, z'_n, z''_1, \dots, z''_m) = -\frac{1}{n} \sum_{i=1}^n z_i'^T z_i'' + \frac{\rho}{n} \sum_{i=1}^n z_i'^T \left(\frac{1}{m} \sum_{j=1}^m z_j'' z_j''^T \right) z_i' \quad (9)$$

$$= -\frac{1}{n} \sum_{i=1}^n z_i'^T z_i'' + \frac{\rho}{n} \sum_{i=1}^n z_i'^T C_t z_i' \quad (10)$$

where $C_t = \frac{1}{m} \sum_{j=1}^m z_j'' z_j''^T$ at step t .

Therefore, instead of saving each vector z_j'' , which requires memory size $O(md)$, we only need to save the matrix C_t that needs memory size $O(d^2)$. However, simply replacing the memory bank with the matrix C_t will not work, as it's not obvious how to remove the old embeddings without storing all the C_t matrices from previous m/n steps. Here, we can apply the same idea of the momentum encoder, and change the matrix C_t from actual average of past m/n batches to an exponential moving average of the outer product $z_j'' z_j''^T$ as follows:

$$C_t = \begin{cases} \mathbf{0}, & t = 0 \\ \beta C_{t-1} + (1 - \beta) \frac{1}{n} \sum_{i=1}^n z_i'' z_i''^T, & \text{otherwise} \end{cases} \quad (11)$$

After changing the actual average to the exponential moving average, we recover the loss function from equation 4 used by TiCo. One difference is that TiCo uses $z' z'^T$ to update the C_t , instead of $z'' z''^T$. That is because, based on our experiments, using $z' z'^T$ produces a slightly better performance

than using $z'' z''^T$. We leave the analysis of the difference between the two choices as one future work.

The analysis above shows that TiCo is implicitly a contrastive learning method. Using the momentum encoder and the exponential moving covariance matrix helps avoiding the necessity of a large batch size or a large memory bank.

3.3 TiCo as a Redundancy-Reduction Method

It can be shown that TiCo is also a redundancy-reduction method by demonstrating the similarities between the squared contrastive loss and the loss function used by Barlow Twins. To simplify the discussion, we assume $\theta = \xi$, i.e. that the two encoders are identical.

Let $Z' \in \mathbb{R}^{d \times n}$ be a matrix where i -th column is z'_i , and $Z'' \in \mathbb{R}^{d \times n}$ be a matrix where i -th column is z''_i . Let Z'_F be the matrix Z' normalized along the feature dimension, and Z'_B be the matrix Z' normalized along the batch dimension. Then both $\text{Tr}(Z'^T_F Z'_F) = n$ and $\text{Tr}(Z'^T_B Z'_B) = d$ are constants.

The squared contrastive loss and the loss function used by Barlow Twins are essentially connected through the following results:

Remark 3.1. Given an embedding matrix $Z \in \mathbb{R}^{d \times n}$, the covariance matrix $C = ZZ^T$ and the Gram matrix $K = Z^T Z$ have the following properties:

1. C and K share the same nonzero eigenvalues $\lambda_1, \dots, \lambda_r$, where r is the rank of the C and K
2. $\text{Tr}(C) = \text{Tr}(K) = \sum_{i=1}^{\min(n,d)} \lambda_i$
3. $\sum_{i=1}^d \sum_{j=1}^d C_{ij}^2 = \|C\|_F^2 = \|K\|_F^2 = \sum_{i=1}^n \sum_{j=1}^n K_{ij}^2 = \sum_{i=1}^{\min(n,d)} \lambda_i^2$

These are known results of linear algebra, but we give simple proofs in the Appendix.

Since $\theta = \xi$, we can see that z'_j and z''_j have the same distribution. Then, we can substitute all $z_i'^T z_j''$ with $z_i'^T z_j'$ without changing the loss function when $i \neq j$.

Now, we have:

$$\ell_{\text{Squared}}(Z'_F, Z''_F) = -\frac{1}{n} \sum_{i=1}^n z_i'^T z_i'' + \frac{\rho}{n} \sum_{i=1}^n \sum_{j=1, j \neq i}^n (z_i'^T z_j')^2 \quad (12)$$

$$= -\frac{1}{n} \text{Tr}(Z'^T_F Z''_F) - \rho + \frac{\rho}{n} \|K_F\|_F^2 \quad (13)$$

$$= -\frac{1}{n} \text{Tr}(Z'^T_F Z''_F) - \rho + \frac{\rho}{n} \|C_F\|_F^2 \quad (14)$$

which shows that the loss function is trying to minimize the Frobenius norm of the covariance matrix $\|C_F\|_F^2$. Furthermore, we have:

$$\|C_F\|_F^2 = \sum_{i=1}^d \lambda_i^2 \quad \text{and} \quad \sum_{i=1}^d \lambda_i = n \quad (15)$$

By Cauchy–Schwarz inequality, we have:

$$\left(\sum_{i=1}^d \lambda_i \right)^2 \leq \left(\sum_{i=1}^d \lambda_i^2 \right) * \left(\sum_{i=1}^d 1^2 \right) \quad (16)$$

$$\sum_{i=1}^d \lambda_i^2 \geq \frac{n^2}{d} \quad (17)$$

Hence, the lower bound of $\|C_F\|_F^2$ is $\frac{n^2}{d}$. It reaches the lowest value when $\lambda_i = \frac{n}{d}, \forall i = \{1, \dots, d\}$, which means C_F is a scaled identity matrix $\frac{n}{d} I$. Then, by minimizing the negative part of the squared

contrastive loss, we are optimizing the covariance matrix $Z_F Z_F^T$ to be as close as possible to a scaled identity matrix, in which all the off-diagonal terms are 0, and all the diagonal terms are equal. Therefore the redundancy-reduction principle [2] used to justify Barlow Twins [35] can also be applied to the loss function of TiCo.

3.3.1 The Loss Function of Barlow Twins

Barlow Twins [35] has the following loss function:

$$\ell_{\text{Barlow}}(Z'_B, Z''_B) = \frac{1}{d} \sum_{i=1}^d (1 - (C'_B)_{ii})^2 + \frac{\rho}{d} \sum_{i=1}^d \sum_{j=1, j \neq i}^d (C'_B)_{ij}^2 \quad (18)$$

where $C'_B = Z'_B Z''_B^T$.

We can do an expansion to the loss function with replacing C'_B with $C_B = Z'_B Z'_B^T$ in the second term of equation 18, so we have:

$$\ell_{\text{Barlow}}(Z'_B, Z''_B) = 1 + \frac{1}{d} \sum_{i=1}^d (C'_B)_{ii}^2 - \frac{2}{d} \sum_{i=1}^d (C'_B)_{ii} + \frac{\rho}{d} \sum_{i=1}^d \sum_{j=1, j \neq i}^d (C_B)_{ij}^2 \quad (19)$$

$$= 1 + \frac{1}{d} \sum_{i=1}^d (C'_B)_{ii}^2 - \frac{2}{d} \text{Tr}(Z'_B{}^T Z''_B) - \rho + \frac{\rho}{d} \|C_B\|_F^2 \quad (20)$$

It is easy to see that there are only two differences between the loss functions in equation 14 and equation 20. The first difference is the term $\frac{1}{d} \sum_{i=1}^d (C'_B)_{ii}^2$. It can be considered as another regularization term for the covariance matrix, which will not change the optimization objective. The second difference is the direction of the normalization. Squared contrastive loss function uses vectors normalized along the feature dimension and the Barlow twins uses values normalized along the batch dimension. We discuss the effect of the normalization in Section 5.

The similarity of TiCo’s loss function and the loss function used by Barlow Twins [35] further justify the claim that TiCo is a redundancy-reduction method. Adding the momentum encoder and the exponential moving covariance matrix to our method improves redundancy reduction by decorrelating channels across batches.

3.4 Implementation Details

Image augmentations We use the same augmentation as used in BYOL [15]. We transform each input image with two sampled augmentations to produce two distorted versions of the input. The augmentation pipeline consists of random cropping, resizing to 224×224 , randomly flipping the images horizontally, applying color distortion, optionally converting to grayscale, adding Gaussian blurring, and applying solarization.

Architecture The encoder f_θ is a ResNet-50 model [18] without final linear layer. The projector g_θ consists of two linear layers, one with 4096 output units and the other with 256 output units. We add batch normalization and ReLU between the two linear layers.

Optimization We closely follow the optimization protocol of BYOL [15]. We use the LARS optimizer [34]. The training schedule starts with a warm-up period which linearly increases the learning rate from 0 to 3.2 ($= 0.2 \times \text{batch size}/256$) in the first 10 epochs. Then the learning rate slowly decreases to 0.032 ($= 0.002 \times \text{batch size}/256$) by following cosine decay schedule without restarts. The total number of epochs is 1000. Weight decay parameter is set to $1.5 \cdot 10^{-6}$. Weight decay and LARS adaptation are not applied to the biases and batch normalization parameters.

4 Results

In order to assess our model’s performance, we have used a similar testing regime to Barlow Twins [35]. The training set images of the ImageNet ILSVRC-2012 dataset [8] are used, without labels,

Table 1: **Linear evaluation — top-1 and top-5 accuracies (in %), when using a linear classifier on representations. Semi-supervised learning — top-1 and top-5 accuracies (in %) when using either 1% or 10% of the dataset for training.** All experiments used the validation set of ImageNet. All models used a ResNet-50 architecture as encoder.

Method	Linear Evaluation		Semi Supervised			
	Top-1	Top-5	Top-1		Top-5	
			1%	10%	1%	10%
Supervised	76.5		25.4	56.4	48.4	80.4
MoCo	60.6					
PIRL	63.6				57.2	83.8
SimCLR	69.3	89.0	48.3	65.6	75.5	87.8
MoCo v2	71.1	90.1				
SimSiam	71.3					
SwAV	71.8					
Barlow Twins	73.2	91.0	55.0	69.7	79.2	89.3
BYOL	74.3	91.6	53.2	68.8	78.4	89.0
SwAV (with multi-crop)	75.3		53.9	70.2	78.5	89.9
TiCo (ours)	73.4	91.6	53.0	66.8	79.2	88.0

Table 2: **Linear classification using image representations produced by a model pretrained with TiCo.** Note that the representations are fixed during training. For Places-205 and iNat18, top-1 accuracy (in %) is reported. For VOC07, the mAP is reported.

Method	Places-205	VOC07	iNat18
Supervised	53.2	87.5	46.7
SimCLR	52.5	85.5	37.2
MoCo v2	51.8	86.4	38.6
SwAV	52.8	86.4	39.5
Barlow Twins	54.1	86.2	46.5
BYOL	54.0	86.6	47.6
SwAV (with multi-crop)	56.7	88.9	48.6
TiCo (ours)	54.0	86.5	45.1

for self-supervised training of our model, following the procedures described in the previous section. Later the pretrained model evaluated for different tasks, as proposed by [14]. In the first experiment, the representations produced by this pretrained encoder are given as input to a linear classifier. In the second experiment, we assess the model’s performance with a reduced amount of training data, in a semi-supervised fashion. Experiments 3 and 4 apply the pretrained model to different datasets for classification, object detection and instance segmentation tasks.

ImageNet: Linear Evaluation and Semi-Supervised Learning For the linear evaluation experiment, we use a ResNet-50 that is pretrained with TiCo to produce representations of the images in the ImageNet dataset, which are then fed into a linear classifier. For the semi-supervised learning experiments, we sample a subset of images from the ImageNet dataset, either 1% or 10% , and use them to fine-tune a ResNet-50 that was pretrained using TiCo. In Table 1 we show the top-1 and top-5 accuracies of ours and other state-of-the-art models for each of the experiments.

Fixed Representations for Image Classification on Multiple Datasets We use a model pretrained with TiCo on ImageNet to produce image representations on a set of other datasets, which are used for training a linear classifier, as suggested by [20]. This was evaluated on Places-205 [38], VOC07 [11] and iNaturalist2018 [30]. In Table 2 we show the accuracies (in %) achieved in each dataset.

Object Detection and Instance Segmentation on Multiple Datasets We have followed the procedures in [16] to produce representations for object detection and instance segmentation tasks. In

Table 3: **Object detection and instance segmentation on multiple datasets** We apply a model that is pretrained on ImageNet with TiCo to produce image representations that are used to perform object detection on VOC07+12 and COCO, and instance segmentation on COCO. The object detection task uses Faster R-CNN and the instance segmentation task uses Mask R-CNN, both with the FPN backbone [33] and the 1x learning rate schedule.

Method	VOC07+12 det			COCO det			COCO instance seg		
	AP _{all}	AP ₅₀	AP ₇₅	AP ^{bb}	AP ₅₀ ^{bb}	AP ₇₅ ^{bb}	AP ^{mk}	AP ₅₀ ^{mk}	AP ₇₅ ^{mk}
Supervised	53.5	81.3	58.8	38.2	58.2	41.2	33.3	54.7	35.2
MoCo v2	57.4	82.5	64.0	39.3	58.9	42.5	34.4	55.8	36.5
SwAV	56.1	82.6	62.7	38.4	58.6	41.3	33.8	55.2	35.9
SimSiam	57.0	82.4	63.7	39.2	59.3	42.1	34.4	56.0	36.7
Barlow Twins	56.8	82.6	63.4	39.2	59.0	42.5	34.3	56.0	36.5
TiCo (ours)	56.2	83.1	62.3	37.4	57.9	41.0	34.5	55.2	37.3

table Table 3 we present the results on VOC07+12 [11] and COCO [19]. In this case, note that the models are fine-tuned during training.

5 Discussion

5.1 The Effect of Normalization

In Section 3.3, the normalization can be considered equivalent to adding an equality constraint to the following optimization problem:

$$\text{minimize } \sum_i \lambda_i^2 \quad (21)$$

$$\text{subject to } \sum_i \lambda_i = 1 \quad (22)$$

Normalizing along the feature dimension or the batch dimension will both result in the same equality constraint, despite having different sets of eigenvalues. Without this constraint, the optimization will lead to the trivial solution that $\sum_i \lambda_i^2 = 0$.

Recently proposed method VICReg [1] doesn’t need normalization, since it adds a hinge loss on the standard deviation. Because the sum of per channel variance is the sum of eigenvalues of the covariance matrix, VICReg can avoid the trivial solution that $\sum_i \lambda_i^2 = 0$ by adding a penalty that prevents the sum of eigenvalues from becoming too small.

5.2 Gram matrix and Covariance Matrix

Roughly speaking, we can consider contrastive losses as functions defined on the Gram matrix of the embeddings, and the loss functions used by redundancy reduction methods to be functions defined on the covariance matrix of the embeddings.

The Gram matrix and covariance matrix always share the same eigenvalues. Therefore, all redundancy reduction methods that only depend on the eigenvalues of the covariance matrix can be thought of contrastive learning methods in general, and contrastive learning methods that only depend on the eigenvalues of the Gram matrix can be considered redundancy reduction methods.

The understanding of the described duality of the Gram matrix and covariance matrix may lead to better designs of loss functions for joint embedding methods.

6 Conclusion

In this paper, we have presented TiCo, a self-supervised learning method for visual representation learning. Despite its simplicity, it achieves similar performance to other state-of-the-art joint

embedding methods in multiple tasks and datasets. We also provide a theoretical explanation of its underlying mechanism. It can be categorized as both a contrastive learning and a redundancy reduction method. Lastly, we show that the two types of methods are closely interconnected through the relationship between the Gram matrix and the covariance matrix of the embeddings.

References

- [1] A. Bardes, J. Ponce, and Y. LeCun. Vicreg: Variance-invariance-covariance regularization for self-supervised learning. *arXiv preprint arXiv:2105.04906*, 2021.
- [2] H. B. Barlow et al. Possible principles underlying the transformation of sensory messages. *Sensory communication*, 1(01), 1961.
- [3] M. Caron, P. Bojanowski, A. Joulin, and M. Douze. Deep clustering for unsupervised learning of visual features. In *Proceedings of the European Conference on Computer Vision (ECCV)*, pages 132–149, 2018.
- [4] M. Caron, I. Misra, J. Mairal, P. Goyal, P. Bojanowski, and A. Joulin. Unsupervised learning of visual features by contrasting cluster assignments. *arXiv preprint arXiv:2006.09882*, 2020.
- [5] T. Chen, S. Kornblith, M. Norouzi, and G. Hinton. A simple framework for contrastive learning of visual representations. In *International conference on machine learning*, pages 1597–1607. PMLR, 2020.
- [6] X. Chen and K. He. Exploring simple siamese representation learning. *arXiv preprint arXiv:2011.10566*, 2020.
- [7] S. Chopra, R. Hadsell, and Y. LeCun. Learning a similarity metric discriminatively, with application to face verification. In *2005 IEEE Computer Society Conference on Computer Vision and Pattern Recognition (CVPR’05)*, volume 1, pages 539–546. IEEE, 2005.
- [8] J. Deng, W. Dong, R. Socher, L.-J. Li, K. Li, and L. Fei-Fei. Imagenet: A large-scale hierarchical image database. In *2009 IEEE conference on computer vision and pattern recognition*, pages 248–255. Ieee, 2009.
- [9] C. Doersch, A. Gupta, and A. A. Efros. Unsupervised visual representation learning by context prediction. In *Proceedings of the IEEE international conference on computer vision*, pages 1422–1430, 2015.
- [10] A. Dosovitskiy, J. T. Springenberg, M. Riedmiller, and T. Brox. Discriminative unsupervised feature learning with convolutional neural networks. *Advances in neural information processing systems*, 27, 2014.
- [11] M. Everingham, L. Van Gool, C. K. Williams, J. Winn, and A. Zisserman. The pascal visual object classes (voc) challenge. *International journal of computer vision*, 88(2):303–338, 2010.
- [12] P. Goyal, P. Dollár, R. Girshick, P. Noordhuis, L. Wesolowski, A. Kyrola, A. Tulloch, Y. Jia, and K. He. Accurate, large minibatch sgd: Training imagenet in 1 hour. *arXiv preprint arXiv:1706.02677*, 2017.
- [13] P. Goyal, Q. Duval, J. Reizenstein, M. Leavitt, M. Xu, B. Lefaudeaux, M. Singh, V. Reis, M. Caron, P. Bojanowski, A. Joulin, and I. Misra. Vissl. <https://github.com/facebookresearch/vissl>, 2021.
- [14] P. Goyal, D. Mahajan, A. Gupta, and I. Misra. Scaling and benchmarking self-supervised visual representation learning. In *Proceedings of the IEEE/CVF International Conference on Computer Vision*, pages 6391–6400, 2019.
- [15] J.-B. Grill, F. Strub, F. Altché, C. Tallec, P. H. Richemond, E. Buchatskaya, C. Doersch, B. A. Pires, Z. D. Guo, M. G. Azar, et al. Bootstrap your own latent: A new approach to self-supervised learning. *arXiv preprint arXiv:2006.07733*, 2020.
- [16] K. He, H. Fan, Y. Wu, S. Xie, and R. Girshick. Momentum contrast for unsupervised visual representation learning. In *Proceedings of the IEEE/CVF Conference on Computer Vision and Pattern Recognition*, pages 9729–9738, 2020.
- [17] K. He, G. Gkioxari, P. Dollár, and R. Girshick. Mask r-cnn. In *Proceedings of the IEEE international conference on computer vision*, pages 2961–2969, 2017.

- [18] K. He, X. Zhang, S. Ren, and J. Sun. Deep residual learning for image recognition. In *Proceedings of the IEEE conference on computer vision and pattern recognition*, pages 770–778, 2016.
- [19] T.-Y. Lin, M. Maire, S. Belongie, J. Hays, P. Perona, D. Ramanan, P. Dollár, and C. L. Zitnick. Microsoft coco: Common objects in context. In *European conference on computer vision*, pages 740–755. Springer, 2014.
- [20] I. Misra and L. v. d. Maaten. Self-supervised learning of pretext-invariant representations. In *Proceedings of the IEEE/CVF Conference on Computer Vision and Pattern Recognition*, pages 6707–6717, 2020.
- [21] M. Noroozi and P. Favaro. Unsupervised learning of visual representations by solving jigsaw puzzles. In *European conference on computer vision*, pages 69–84. Springer, 2016.
- [22] A. v. d. Oord, Y. Li, and O. Vinyals. Representation learning with contrastive predictive coding. *arXiv preprint arXiv:1807.03748*, 2018.
- [23] S. Ozair, C. Lynch, Y. Bengio, A. v. d. Oord, S. Levine, and P. Sermanet. Wasserstein dependency measure for representation learning. *arXiv preprint arXiv:1903.11780*, 2019.
- [24] D. Pathak, R. Girshick, P. Dollár, T. Darrell, and B. Hariharan. Learning features by watching objects move. In *Proceedings of the IEEE Conference on Computer Vision and Pattern Recognition*, pages 2701–2710, 2017.
- [25] D. Pathak, P. Krahenbuhl, J. Donahue, T. Darrell, and A. A. Efros. Context encoders: Feature learning by inpainting. In *Proceedings of the IEEE conference on computer vision and pattern recognition*, pages 2536–2544, 2016.
- [26] B. Poole, S. Ozair, A. Van Den Oord, A. Alemi, and G. Tucker. On variational bounds of mutual information. In *International Conference on Machine Learning*, pages 5171–5180. PMLR, 2019.
- [27] S. Qiao, H. Wang, C. Liu, W. Shen, and A. Yuille. Micro-batch training with batch-channel normalization and weight standardization. *arXiv preprint arXiv:1903.10520*, 2019.
- [28] S. Ren, K. He, R. Girshick, and J. Sun. Faster r-cnn: towards real-time object detection with region proposal networks. *IEEE transactions on pattern analysis and machine intelligence*, 39(6):1137–1149, 2016.
- [29] Y.-H. H. Tsai, M. Q. Ma, M. Yang, H. Zhao, L.-P. Morency, and R. Salakhutdinov. Self-supervised representation learning with relative predictive coding. *arXiv preprint arXiv:2103.11275*, 2021.
- [30] G. Van Horn, O. Mac Aodha, Y. Song, Y. Cui, C. Sun, A. Shepard, H. Adam, P. Perona, and S. Belongie. The inaturalist species classification and detection dataset. In *Proceedings of the IEEE conference on computer vision and pattern recognition*, pages 8769–8778, 2018.
- [31] P. Vincent, H. Larochelle, Y. Bengio, and P.-A. Manzagol. Extracting and composing robust features with denoising autoencoders. In *Proceedings of the 25th international conference on Machine learning*, pages 1096–1103, 2008.
- [32] X. Wang and A. Gupta. Unsupervised learning of visual representations using videos. In *Proceedings of the IEEE international conference on computer vision*, pages 2794–2802, 2015.
- [33] Y. Wu, A. Kirillov, F. Massa, W.-Y. Lo, and R. Girshick. Detectron2. <https://github.com/facebookresearch/detectron2>, 2019.
- [34] Y. You, I. Gitman, and B. Ginsburg. Large batch training of convolutional networks. *arXiv preprint arXiv:1708.03888*, 2017.
- [35] J. Zbontar, L. Jing, I. Misra, Y. LeCun, and S. Deny. Barlow twins: Self-supervised learning via redundancy reduction. *arXiv preprint arXiv:2103.03230*, 2021.
- [36] R. Zhang, P. Isola, and A. A. Efros. Colorful image colorization. In *European conference on computer vision*, pages 649–666. Springer, 2016.
- [37] R. Zhang, P. Isola, and A. A. Efros. Split-brain autoencoders: Unsupervised learning by cross-channel prediction. In *Proceedings of the IEEE Conference on Computer Vision and Pattern Recognition*, pages 1058–1067, 2017.
- [38] B. Zhou, A. Lapedriza, J. Xiao, A. Torralba, and A. Oliva. Learning deep features for scene recognition using places database. *Advances in neural information processing systems*, 27, 2014.

A Proof of Remark 3.1

Proof.

1. Given an embedding matrix $Z \in \mathbb{R}^{d \times n}$, we can always decompose it using singular value decomposition such that $Z = U\Sigma V^T$, where $U \in \mathbb{R}^{d \times d}$, $\Sigma \in \mathbb{R}^{d \times n}$, $V \in \mathbb{R}^{n \times n}$, U and V are orthogonal matrices, and Σ is a diagonal matrix.

Then we have:

$$C = ZZ^T = U\Sigma V^T V\Sigma^T U^T = U\Sigma\Sigma^T U^T \quad (23)$$

$$K = Z^T Z = V\Sigma^T U^T U\Sigma V^T = V\Sigma^T \Sigma V^T \quad (24)$$

It is easy to see that the columns of U are eigenvectors of C , and the columns of V are eigenvectors of K since we have:

$$Cu_i = (\Sigma\Sigma^T)_{ii}u_i \quad (25)$$

$$Kv_i = (\Sigma^T \Sigma)_{ii}v_i \quad (26)$$

where u_i is i -th column of U and v_i is i -th column of V . The eigenvalues of C and K are the diagonal elements of $\Sigma\Sigma^T$ and $\Sigma^T \Sigma$.

Since Σ is a diagonal matrix, $\Sigma\Sigma^T$ and $\Sigma^T \Sigma$ share the same nonzero diagonal elements. Then C and K share the same nonzero eigenvalues.

2. Since the trace of a matrix is the sum of its eigenvalues, and we already have that C and K share the same nonzero eigenvalues, we have:

$$\text{Tr}(C) = \text{Tr}(K) = \sum_i \lambda_i \quad (27)$$

3. We have the Frobenius norm of matrices C and K equal to:

$$\|C\|_F = \sqrt{\sum_i \sum_j C_{ij}^2} = \sqrt{\sum_i \lambda_i^2} \quad (28)$$

$$\|K\|_F = \sqrt{\sum_i \sum_j K_{ij}^2} = \sqrt{\sum_i \lambda_i^2} \quad (29)$$

Since C and K share the same nonzero eigenvalues, it follows that:

$$\sum_{i=1}^d \sum_{j=1}^d C_{ij}^2 = \|C\|_F^2 = \sum_{i=1}^d \lambda_i^2 = \|K\|_F^2 = \sum_{i=1}^n \sum_{j=1}^n K_{ij}^2 \quad (30)$$

□

B Data Augmentations

For data augmentations, we use the same augmentation parameters as BYOL [15] that are listed in table 4.

Removing Augmentations To examine the effect of removing augmentations, we performed the same ablation studies as proposed in BYOL [15], where all the experiments were done with a batch size of 4096 and for 300 epochs. The experiments show that our method is robust to changes in data augmentations. Without using any data augmentation except random cropping, our model only suffered a 11.3% accuracy drop, which is a significant improvement over SimCLR [5] that suffers a 27.7% accuracy drop using the same setting. The result is listed in table 5.

Table 4: **Data Augmentation Parameters** There are two sets of augmentation parameters. The differences between them are the probabilities of Gaussian blurring and solarization.

Parameter	\mathcal{T}	\mathcal{T}'
Random crop probability	1.0	1.0
Flip probability	0.5	0.5
Color jittering probability	0.8	0.8
Brightness adjustment max intensity	0.4	0.4
Contrast adjustment max intensity	0.4	0.4
Saturation adjustment max intensity	0.2	0.2
Hue adjustment max intensity	0.1	0.1
Color dropping probability	0.2	0.2
Gaussian blurring probability	1.0	0.1
Solarization probability	0.0	0.2

Table 5: **Top-1 accuracies (in %) with different data augmentations** Data for SimCLR and BYOL are from [15]. All the experiments include random flipping data augmentation.

Transformation	BYOL	SimCLR	TiCo
Baseline	72.5	67.9	71.4
No grayscale	70.3	61.9	68.0
No color	63.4	45.7	62.7
Color + blur	61.1	41.7	62.6
Crop only	60.1	40.2	60.1

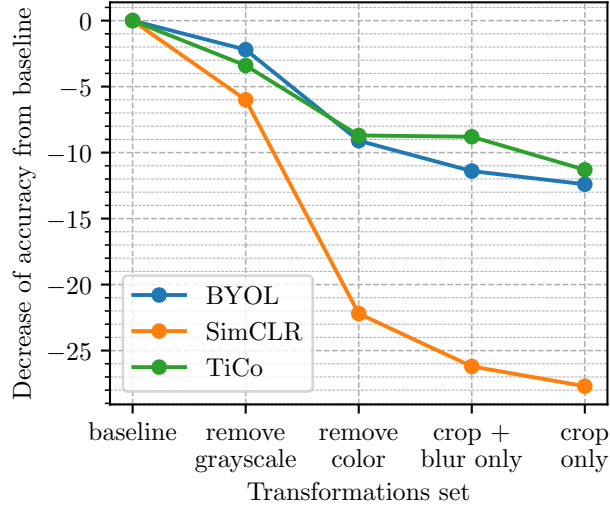


Figure 3: **Impact of progressively removing data augmentations** We show the difference of the top-1 accuracy between using the baseline augmentation and using the simpler augmentation with SimCLR, BYOL and TiCo

C Hyperparameters

C.1 Pretraining

We have trained the final model for 1000 epochs using a batch size of 4096. For the momentum encoder’s hyperparameter α , we increased it from 0.99 to 1.0 using a cosine decay schedule without restarts. During the whole training, the covariance matrix hyperparameter β is fixed to 0.9 and the

weight hyperparameter ρ for the covariance contrast loss is fixed to 8.0. All other hyperparameters are the same as stated in section 3.4.

We also apply the weight standardization trick [27] for all convolution layers to accelerate the convergence of training for experiments with fewer epochs. For 1000 epoch experiments, we don't see a significant improvement over the final accuracy (top-1 accuracy 73.4% with weight standardization and 73.2% without weight standardization).

C.2 Linear Evaluation on ImageNet

We follow the same linear evaluation protocol as in BYOL [15]. We fix the weights of the encoder network. For the linear classifier, we optimize the cross-entropy loss using SGD with Nesterov momentum over 80 epochs using a batch size of 1024, with learning rate 0.4 and momentum 0.9. We do not use weight decay.

C.3 Semi-Supervised Learning on ImageNet

We follow the same semi-supervised learning protocol as in Barlow Twins [35]. We optimize the cross-entropy loss using SGD with Nesterov momentum over 20 epochs using a batch size of 256, with learning rate 0.002 for the encoder network, learning rate 0.5 for the classifier network and momentum 0.9 for both networks. Both learning rates are multiplied by a factor of 0.2 after the 12th and 16th epoch. We do not use weight decay.

C.4 Linear Evaluation on Other Datasets

We follow the same transfer learning evaluation protocol as in PIRL [20]. We fix the weights of the encoder network for all tasks. For Places-205 and iNaturalist2018 we train a linear classifier with SGD (14 epochs on Places-205, 84 epochs on iNaturalist2018) with a learning rate of 0.05 for Places-205 and 4.0 for iNaturalist2018, using an SGD momentum of 0.9 for both. The learning rate of Places-205 is multiplied by a factor of 0.5 after the 4th, 8th and 12th epochs. The learning rate of iNaturalist2018 is multiplied by a factor of 0.1 after the 24th, 48th and 72th epochs. We do not use weight decay for either of the two tasks.

For VOC07 dataset, we train SVM classifiers where the C values are computed using cross-validation.

C.5 Object Detection and Instance Segmentation

We use the VISSL [13] and detectron2 [33] libraries for training and evaluating the detection models.

VOC07+12 We use the VOC07+12 *trainval* set for training a Faster R-CNN [28] with FPN backbone for 24000 iterations using a batch size of 16. The initial learning rate for the model is 0.15 which is reduced by a factor of 0.1 after 18000 and 22000 iterations. We also use linear warmup [12] for the first 1000 iterations.

COCO We use the COCO 2017 *train* split to train Mask R-CNN [17] with FPN backbone. We use a learning rate of 0.08 and keep the other parameters the same as in the $1\times$ schedule in detectron2.

D Miscellaneous

D.1 Compute Resources

The majority of our experiments were run using AMD MI50 GPUs. The final pretraining for 1000 epochs takes about 108 hours on 8 nodes, where each node has 8 MI50 GPUs attached. We estimate that the total amount of compute resources used for all the experiments can be roughly approximated by $75 \text{ (days)} \times 24 \text{ (hours per day)} \times 8 \text{ (nodes)} \times 8 \text{ (GPUs per nodes)} = 115,200 \text{ (GPU hours)}$.

We are aware of potential environmental impact of consuming a lot of compute resources needed for this work, such as atmospheric CO_2 emissions due to the electricity used by the servers. However, we also believe that advancements in self-supervised learning and representation learning can potentially help mitigate these effects by reducing the need for data and compute resources in the future.

D.2 Limitation of Experiment Results

Due to a lack of compute resources, we were not able to conduct a large number of experiments with the goal of tuning hyperparameters and searching for the best configurations. Therefore, the majority of hyperparameters and network configurations used in this work are the same as provided by BYOL [15] or Barlow Twins [35]. The only hyperparameters that were more carefully tuned were ρ , the weight of the covariance contrast loss and β , which controls the update of the covariance matrix. All the other hyperparameters may not be optimal.

In addition, all models were pretrained on the ImageNet [8] dataset, so their performances might differ if pretrained with other datasets containing different data distributions or different types of images (e.g., x-rays). We encourage further exploration in this direction for current and future self-supervised learning frameworks.